Table 1. Clinical features of the subjects

Feature	Cancer	Control†	Metroptosis	Myoma	Healthy
Number of cases	92	33	16	74	17
Mean age ± SD (years)	59.4 ± 10.5	50.8 ± 18.5	65.8 ± 9.8	48.8 ± 4.1	36.7 ± 12.5
Surgical stage‡					
0 (%)	6 (6.50%)				
I (%)	63 (68.5%)				
II (%)	8 (8.70%)				
III (%)	13 (14.1%)				
IV (%)	2 (2.20%)				

†The controls (n = 33) consisted of the metroptosis patients (n = 16) and healthy volunteers (n = 17). ‡Classified according to the 2nd edition of *The General Rules for Clinical and Pathological Management of Uterine Corpus Cancer.*[18]

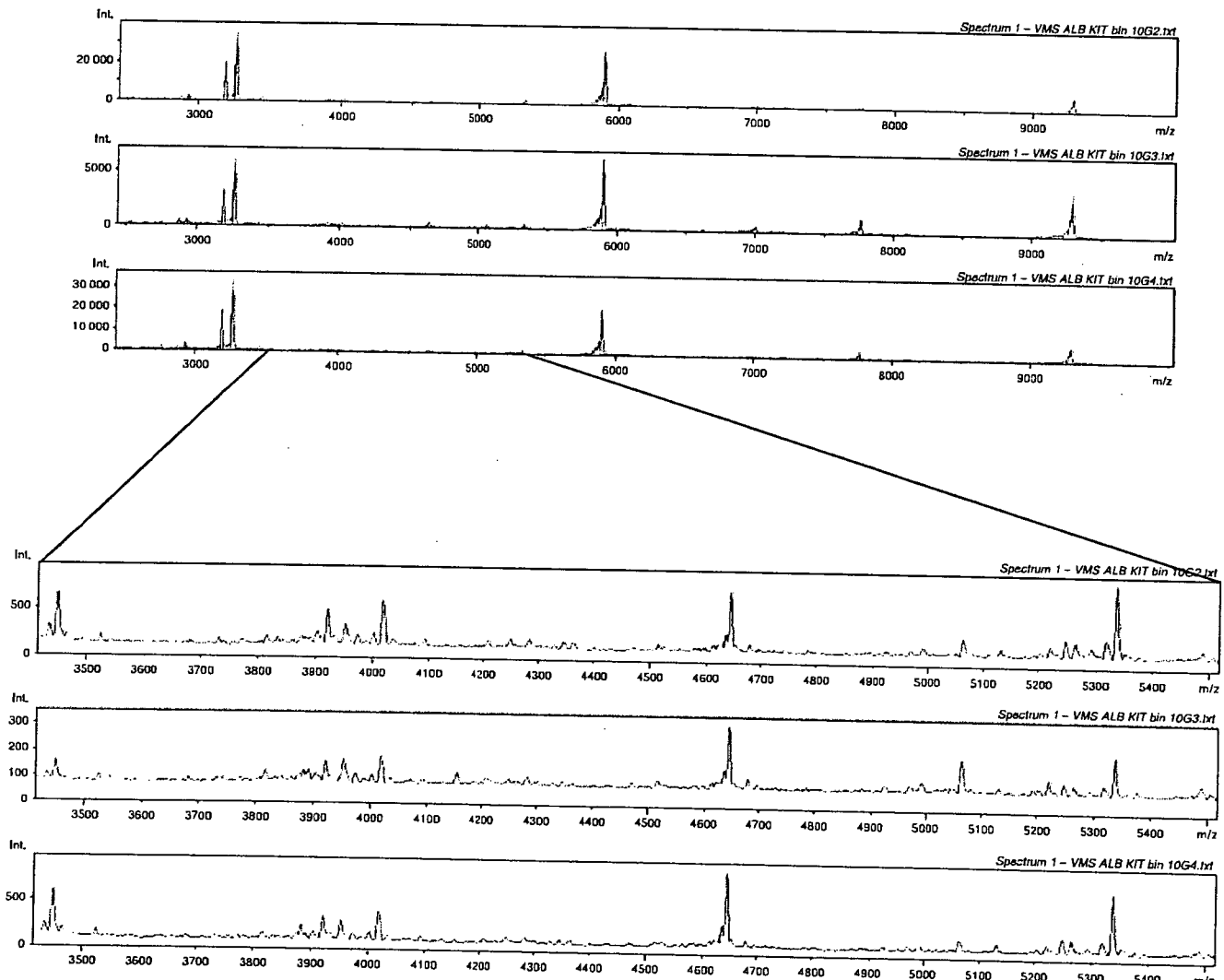

Fig. 1. Direct profiling of serum albumin-associated peptides by matrix-assisted laser desorption/ionization hybrid quadrupole time-of-flight mass spectrometry. Mass spectra of triplicate preparations of serum albumin-associated peptides from a representative healthy volunteer are shown in the ranges of 2500–10 000 m/z (top) and 3400–5500 m/z (bottom).

(PerkinElmer), and the 400-μL diluted serum sample was loaded onto a spin column and spun at 200 *g* for 10 min. The column was washed with binding buffer three times. The sample was desalted with ZipPlate C-18 (Millipore, Bedford, MA, USA) and spotted directly onto a disposable MALDI plate (PerkinElmer) with CHCA (Ciphergen Biosystems, Fremont, CA, USA). Experiments were carried out in triplicate, and only reproducible assays with a correlation coefficient over 0.75 were analyzed further.

MALDI QqTOF-MS. Mass spectra were obtained with a high-resolution orthogonal QqTOF-MS instrument (prOTOF 2000; PerkinElmer). The instrument was set to measure the range between 1000 and 80 000 m/z. Laser shot, laser energy, laser rate, declustering, cooling flow and laser pattern were set at 50,

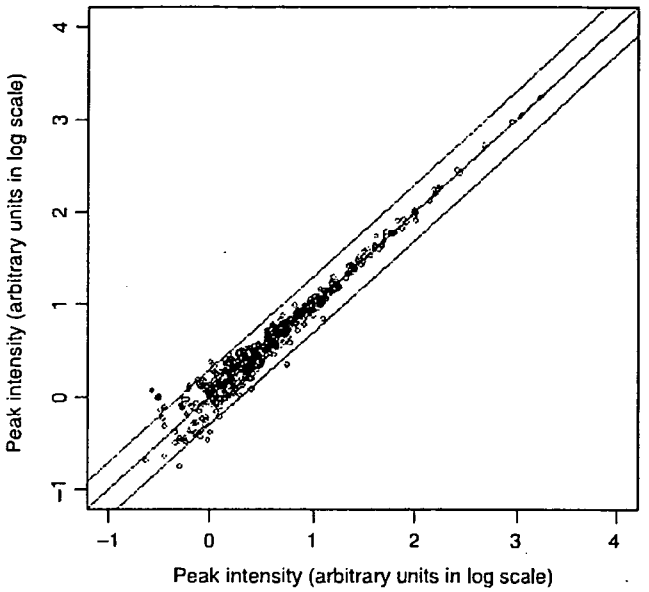

Fig. 2. Reproducibility of profiling of albumin-associated peptides. Two-dimensional plots indicate the high correlation between the relative intensity (in log scale) of corresponding peaks in the duplicate (*x*-axis and *y*-axis) separation and measurements of albumin-associated peptides from a representative serum sample. The correlation coefficient value between the duplicate was 0.975, and 97.83% of the peaks were plotted within a two-fold difference (solid lines).

84%, 29.0 Hz, 30 V, 150.0 mL/min and 2 mm ring 96 spot, respectively. After mass calibration the mass data were converted to text files consisting of m/z and peak intensity. The text files were processed with in-house peak detection, normalization and quantification software (called NCC-ProteoJudge)[19,20] and the peak data were visualized with Mass Navigator software (Mitsui Knowledge Industry, Tokyo, Japan). Mass accuracy was calibrated externally on the day of the measurements with an all-in-one peptide molecular mass standard (Ciphergen Biosystems).

Statistical analysis. Statistically significant differences were detected using the Mann–Whitney *U*-test. ROC curves were generated and AUC values were calculated using StatFlex software (version 5.0; Artech, Osaka, Japan).[21]

ELISA of CA125. The serum CA125 value was measured with a commercial ELISA kit (Elecsys CA125 II reagent kit; Roche Diagnostics, Mannheim, Germany) according to the instructions provided by the supplier.

Results

Detection and quantification of serum albumin-associated peptides. A total of 507 unique serum albumin-bound peptide peaks were detected constantly in the range between 2000 and 30 000 m/z across 125 serum samples (92 endometrial cancer patients and 33 controls) by MALDI QqTOF-MS. Detection and quantification of the peptides was highly reproducible as revealed by visual inspection (Fig. 1) and by calculating the CC of triplicate separation and measurements in every sample (Fig. 2). The mean CC ± SD for the 507 peaks in the 125 serum samples was 0.979 ± 0.035. Reliable quantification seems possible in the range exceeding 10^3 (Fig. 2).

Selection of peptides associated with endometrial cancer. We selected mass peaks whose mean intensity in triplicate measurements differed significantly between the 92 endometrial cancer patients and 33 controls based on predefined statistical criteria ($P < 0.00001$, Mann–Whitney *U*-test and AUC value > 0.80). Three peaks at 4769, 6254 and 11 792 m/z (Fig. 3) were found to fulfill the criteria with *P*-values of 8.99E-8, 1.25E-9 and 7.46E-8 (Table 2) as well as AUC values of 0.813, 0.857 and 0.815 (Fig. 4), respectively. Representative mass spectra of the three peptide peaks (one cancer patient and one control) and gel-like images (30 cancer patients and 30 controls) are shown in Fig. 3.

Sensitivity and specificity of the three peptides. The distribution of the intensity of the three peaks is shown in Fig. 5. When the cut-off values were defined as the mean + 2 SD of the values of the 33 control samples (solid lines), the sensitivity of the 4769-, 6254- and 11 792-m/z peaks was 42.4, 38.0 and 47.8%, respectively, and their specificity was 100, 97.0 and 97.0%, respectively (Fig. 5; Table 3). Endometrial cancer could be diagnosed with a sensitivity of 65.2% when at least one of the three peptides exceeded the cut-off value, but specificity remained high (93.9%).

The sensitivity of each marker and of the combination of the three according to the surgical stage of the patients is shown in Table 4. There was no significant difference in the distribution of peak intensity among endometrial cancer patients of different surgical stages (Suppl. Fig. S2). The combination detected 60.3% of early endometrial cancer at stage I (Fig. 6; Table 4).

The levels of the three peptides in sera of myoma uteri patients were lower than those of endometrial cancer patients and higher than those of controls, and the differences were statistically significant (Table 2). When the cut-off values were defined as the mean + 2 SD of the controls, the intensities of the 4769-, 6254-, and 11 792-m/z peaks were above the cut-offs in 31.1 (23/74), 13.5 (10/74) and 24.3% (18/74) of myoma patients, respectively (Fig. 6), indicating that none of the three peptides is specific to endometrial cancer.

Comparison to CA125. CA125 is a known serum marker of endometrial cancer and ovarian cancer.[22] We analyzed the level of CA125 in the serum of the 77 cancer patients and 30 controls whose remaining serum sample was sufficient to make the measurement. When the cut-off value was set at 35 IU/mL, the sensitivity of CA125 was 22.1% (17/77), and its specificity was 90.0% (27/30) (Table 3), indicating that each peptide marker identified in this study as well the combination of the three peptides was superior to CA125 in detecting endometrial cancer. The sensitivity of CA125 was highly dependent on the surgical stage of the cancer, and only 17.3% (9/52) of the stage I cancers were detected with CA125 (Table 4). The reactivity of CA125 and peptide markers in each subject is shown in Fig. 6.

Table 2. Distribution of the 4786-, 6254- and 11 792-m/z peaks

Peaks	Cancer (*n* = 92)	Myoma (*n* = 74)	Control (*n* = 33)	*P*-value*	*P*-value**	*P*-value***
4769 m/z	2.24 ± 0.59†	2.00 ± 0.49†	1.62 ± 0.32†	8.99E-8	1.40E-2	2.67E-4
6254 m/z	3.60 ± 1.16†	3.01 ± 0.96†	2.47 ± 0.56†	1.25E-9	4.72E-5	2.34E-4
11 792 m/z	4.43 ± 2.27†	3.55 ± 2.14†	2.35 ± 0.84†	7.46E-8	4.93E-3	9.80E-5

Mann–Whitney *U*-test between: *cancer patients and controls; **cancer patients and myoma patients; ***myoma patients and controls. †Mean intensity ± SD in arbitrary units.

doi: 10.1111/j.1349-7006.2007.00458.x

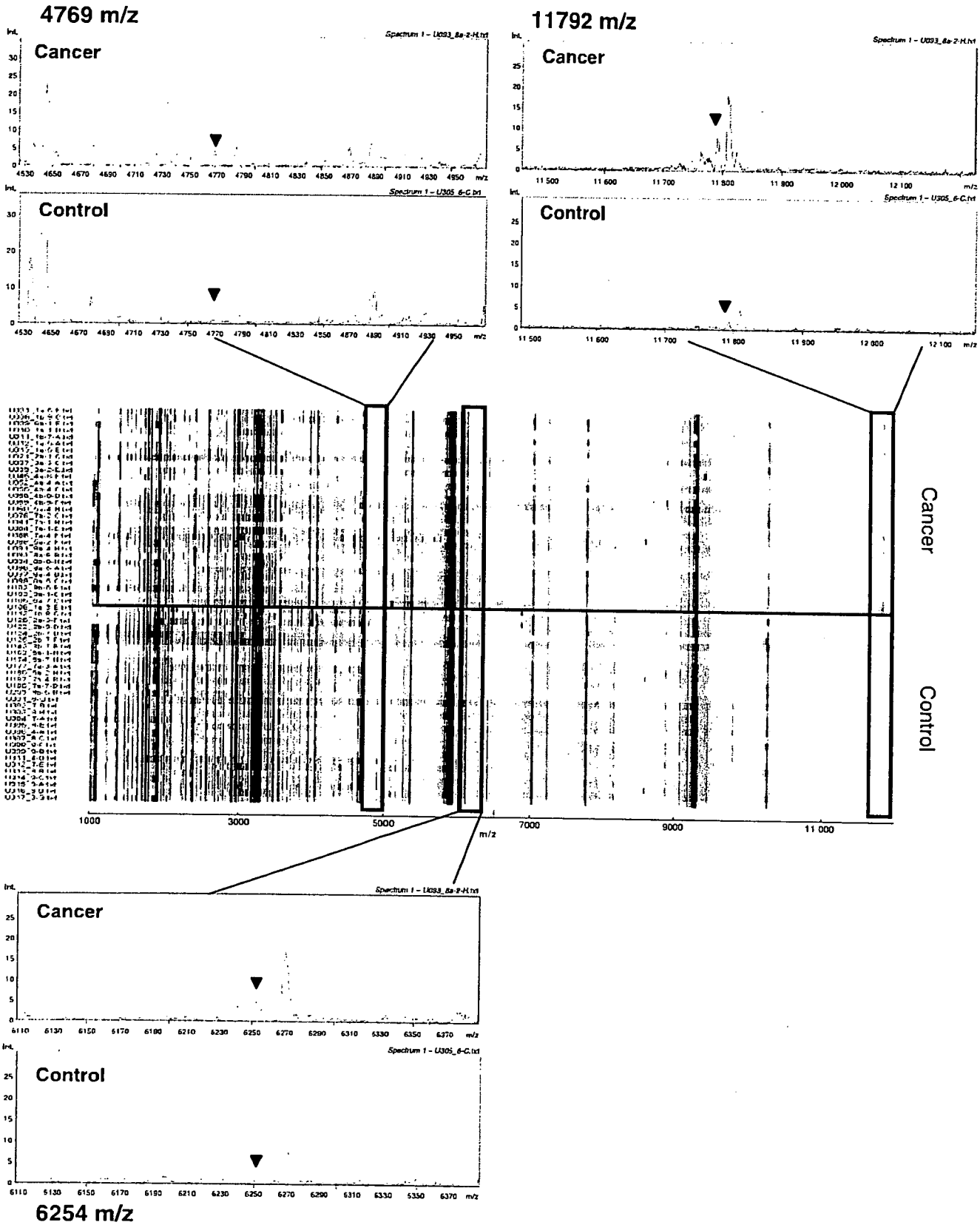

Fig. 3. Marker peptides in the serum of uterine endometrial cancer patients. Representative mass spectra of the serum peptides of a healthy volunteer and an endometrial cancer patient showing the peaks at 4769, 6254 and 11 792 m/z, and gel-like images converted from mass spectra of 30 controls and 30 cancer patients.

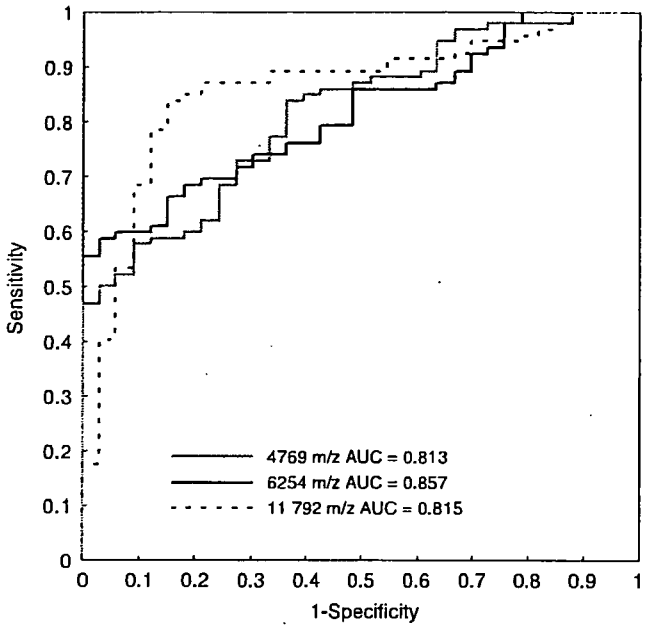

Fig. 4. Receiver operator characteristics analysis of peptides of uterine endometrial cancer. Receiver operator characteristics curves and area under the curve values showing the discrimination capacities of the 4769-, 6254- and 11 792-m/z peaks.

Discussion

Various cytokines, growth factors, ligands, enzymes and their inhibitors are secreted in the local tumor microenvironment and participate in tumor growth, metastasis and angiogenesis. Profiling of circulating serum proteins unquestionably provides useful information for cancer diagnosis. However, direct detection and quantification of biomarkers with low-abundance by mass spectrometry is often complicated by a handful of abundant proteins, including albumin, immunoglobulin and transferrin. Various proteases, including serine proteases and matrix metalloproteinases, are activated during the process of tissue remodeling-associated tumor expansion and invasion, and a large variety of proteolytic fragments are released into the bloodstream. These low molecular weight protein fragments and peptides are bound to large proteins, such as albumin, and are stably retained in the circulation. Lowenthal *et al.* recently analyzed the serum albumin-bound peptides of ovarian cancer patients by ESI-MS coupled with liquid chromatography and identified proteolytic fragments of a tumor suppressor protein, BRCA2 (breast cancer 2).[14] However, the clinical utility of these albumin-associated peptides as cancer tumor markers has not been established. In the present study we demonstrated that a large number of albumin-associated peptides can be detected and quantified reproducibly by high-resolution MALDI QqTOF-MS (Figs 1,2).

The serum of the endometrial cancer patients and control subjects contained a large variety of albumin-associated

Table 3. Sensitivity and specificity of 3 albumin-associated peptides and CA125

	4769 m/z	6254 m/z	11 792 m/z	Combination	CA125
Sensitivity					
%	42.4†	38.0†	47.8†	65.2‡	22.1§
n	39/92	35/92	44/92	60/92	17/77
Specificity					
%	100†	97.0†	97.0†	93.9‡	90.0§
n	33/33	32/33	32/33	31/33	27/30

†Cut-off values were defined as the averages of the values in the controls ($n = 33$) + 2 SD. ‡Any of the three peaks exceeded the cut-offs. §Cut-off was defined as 35 IU/mL.

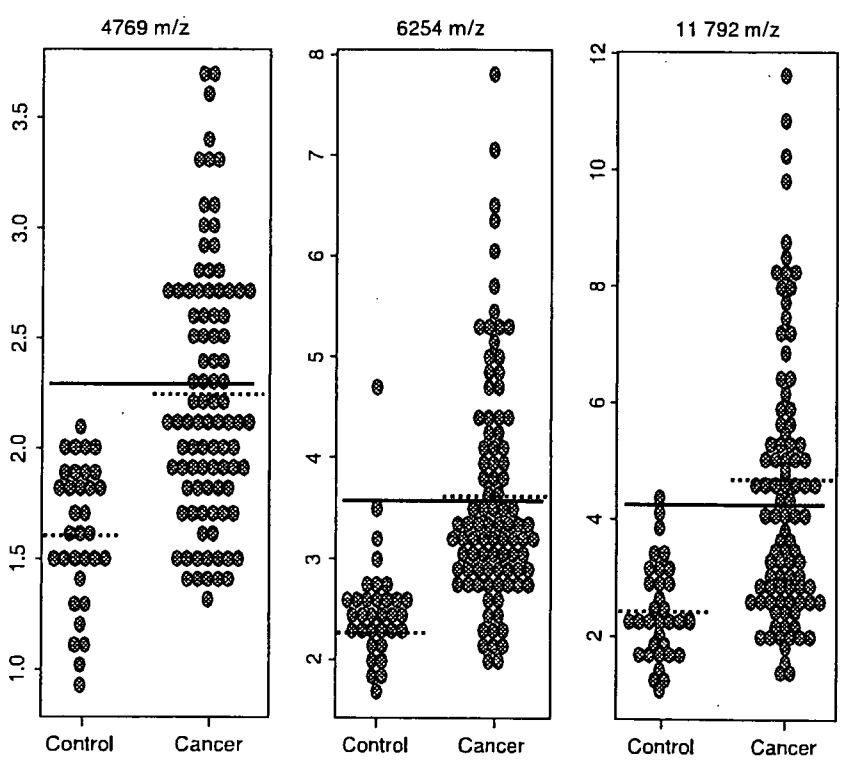

Fig. 5. Scatter graph of the 4769-, 6254- and 11 792 m/z-peaks. The difference in distribution of the intensity of each peak between the controls and cancer patients was statistically significant (Mann–Whitney *U*-test). Solid lines represent the average intensity values of the healthy controls + 2 SD. The broken lines indicate the average intensity in the controls and cancer patients.

doi: 10.1111/j.1349-7006.2007.00458.x

Table 4. Sensitivity according to surgical stage

Surgical stage[†]	4769 m/z		6254 m/z		11 792 m/z		Combination		CA125	
	%	*n*	%	*n*	%	*n*	%	*n*	%	*n*
0	50.0	3/6	33.3	2/6	50.0	3/6	66.7	4/6	0	0/4
I	36.5	23/63	34.9	22/63	42.9	27/63	60.3	38/63	17.3	9/52
II	37.5	3/8	37.5	3/8	75.0	6/8	75.0	6/8	12.5	1/8
III	61.5	8/13	46.2	6/13	46.2	6/13	76.9	10/13	45.5	5/11
IV	100	2/2	100	2/2	100	2/2	100	2/2	100	2/2
Total	42.4	39/92	38.0	35/92	47.8	44/92	65.2	60/92	22.1	17/77

[†]Classified according to the 2nd edition of *The General Rules for Clinical and Pathological Management of Uterine Corpus Cancer.*[18]

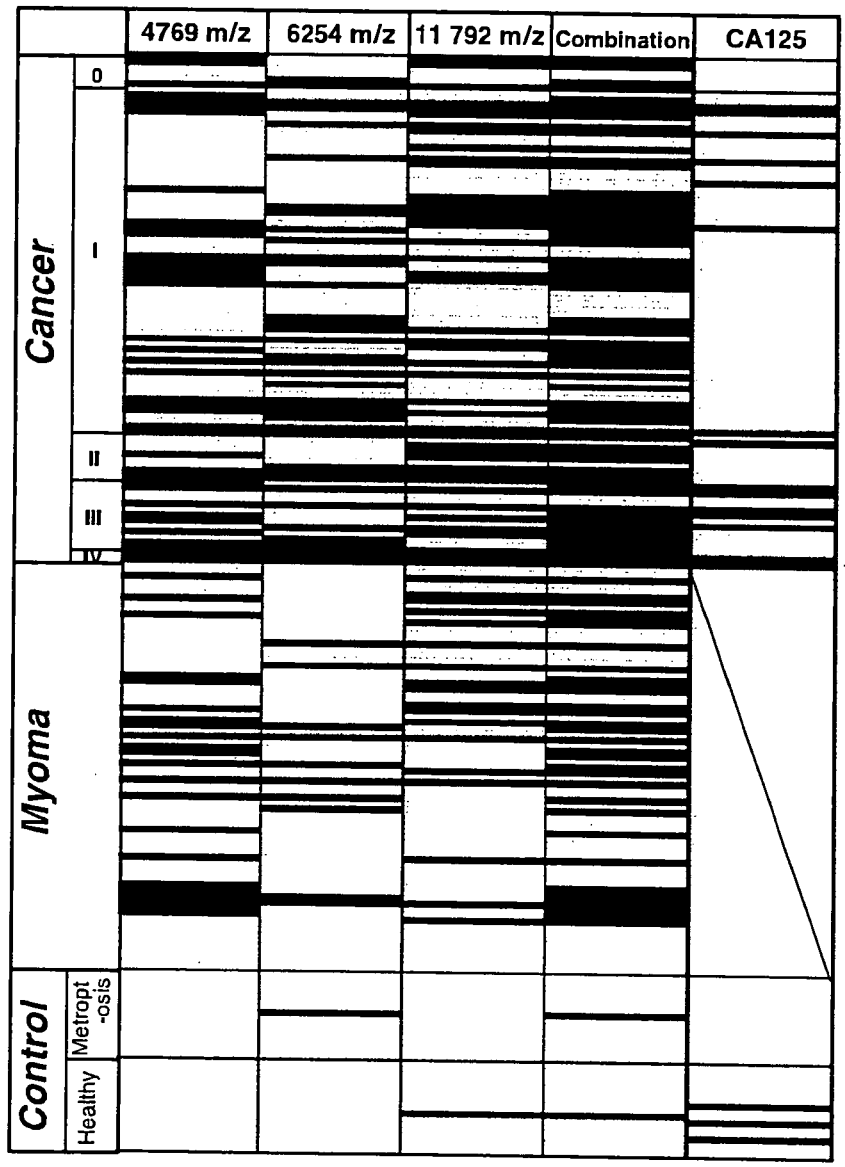

Fig. 6. Comparison of peptides and CA125. Individuals whose values for the single 4769-, 6254- and 11 792-m/z peaks, their combination, and CA125 exceeded the cut-off values are darker. Asterisks, not examined.

peptides, but most peptide peaks did not differ significantly between the controls and endometrial cancer patients (Fig. 3). We used a very strict statistical criterion ($P < 0.00001$, Mann–Whitney U-test) to search for peptides associated with endometrial cancer, because it was estimated that 5 of the 507 detectable peaks would by chance achieve a P-value of 0.01. We found that the intensity of only three peptides differed significantly between the endometrial cancer patients and controls with P-values at the 10^{-8} level (Table 2), meaning that chance identification of these peptides is unlikely.

ROC analysis (Fig. 4) and the distribution of peak intensity (Fig. 5) revealed that these three peaks had high discriminatory

capacity, indicating their potential as novel serum tumor markers of endometrial cancer. CA125 has been one of the most reliable tumor markers for adenocarcinoma of the uterus and is used frequently in clinical settings[23] but the sensitivity (65.2%) of the peptide marker set identified in this study was clearly higher than that of CA125 (22.1%) (Table 3). Furthermore, the marker set detected even early (stage I and II) endometrial cancer with a sensitivity of 60.3 and 75.0%, respectively (Table 4). The serum CA125 level is a prognostic indicator of endometrial cancer, but CA125 has been found to be unsatisfactory for the diagnosis of early stage endometrial cancer. Consistent with the results of this study the CA125 level has been reported to be elevated in only 13–22% of patients with early endometrial cancer.[24,25]

Thus far no attempts to obtain the amino acid sequences of the three albumin-associated peptides identified in this study have been successful, because it was impossible to separate the proteins from these low-abundance peaks by multidimensional liquid chromatography without contamination by neighboring peaks (Fig. 3). The size of the three peptides (4769, 6254 and 11 792 m/z) was beyond the range manageable by the direct tandem MS (MS/MS) of QqTOF-MS. Fourier transform MS may overcome this problem, because it does not require enzymatic digestion and complete purification as preconditions for protein identification. However, the interface to the MALDI is not used for Fourier MS in practice. Furthermore, the identification of circulating blood proteins by MS/MS may not be as straightforward as previously thought, because the inclusion of novel exons and previously nonannotated gene sequences has resulted in computing errors and false identification of plasma proteins.[26] The high reproducibility of QqTOF-MS (Figs 1,2), however, warrants direct application of its measurements to clinical use and does not necessitate actual protein identification of the peaks.

A mass screening program for endometrial cancer has been conducted in Japan since 1987 under the Health and Medical Service Law for the Aged.[27] Although extensive screening by endometrial cytology is expected to increase the rate of detection of early endometrial cancer and improve the overall survival rate,[28] only 5–6% of the eligible population of women enrolled in the mass screening program, probably because of shame and fear of the pain and complications associated with the cytological examination. The introduction of an effective blood test into mass screening for endometrial cancer might lower the psychological hurdle and increase enrolment dramatically. However, the current peptide marker set seems insufficient for its application to mass screening because of the high prevalence of asymptomatic myoma uteri in the general population. Its use might be limited to ambulatory gynecologic practice as a safe option to reduce the chance of missing asymptomatic endometrial cancer and myoma cases for which cytological and ultrasound examinations give negative results.

Although a confirmatory study will be necessary to verify the diagnostic accuracy of the peptides, our data clearly indicate the feasibility of direct profiling of albumin-associated peptides for tumor marker discovery.

Acknowledgments

We thank Mr H. Kuwabara, Mr T. Sakuma, and Ms M. Sato of the Mitsui Knowledge Industry Co. (Tokyo, Japan) for the statistical analyses, and Mr S. Sagara of PerkinElmer Japan (Tokyo, Japan) for technical assistance. S. Kikuchi is the recipient of a 'Research Resident Fellowship' from the Foundation for the Promotion of Cancer Research (Tokyo, Japan). This study was supported by grants from the Ministry of Health, Labor and Welfare of Japan, the Ministry of Education, Culture, Sports, Science and Technology of Japan, the National Institute of Biomedical Innovation of Japan, and the Naito Foundation.

References

1 Kuwabara Y, Susumu N, Banno K *et al.* Clinical characteristics of prognostic factors in poorly differentiated (G3) endometrioid adenocarcinoma in Japan. *Jpn J Clin Oncol* 2005; **35**: 23–7.
2 Armstrong B, Doll R. Environmental factors and cancer incidence and mortality in different countries, with special reference to dietary practices. *Int J Cancer* 1975; **15**: 617–31.
3 Zeleniuch-Jacquotte A, Akhmedkhanov A, Kato I *et al.* Postmenopausal endogenous oestrogens and risk of endometrial cancer: results of a prospective study. *Br J Cancer* 2001; **84**: 975–81.
4 Calle EE, Rodriguez C, Walker-Thurmond K, Thun MJ. Overweight, obesity, and mortality from cancer in a prospectively studied cohort of US adults. *N Engl J Med* 2003; **348**: 1625–38.
5 Anderson KE, Anderson E, Mink PJ *et al.* Diabetes and endometrial cancer in the Iowa women's health study. *Cancer Epidemiol Biomarkers Prev* 2001; **10**: 611–16.
6 Furberg AS, Thune I. Metabolic abnormalities (hypertension, hyperglycemia and overweight), lifestyle (high energy intake and physical inactivity) and endometrial cancer risk in a Norwegian cohort. *Int J Cancer* 2003; **104**: 669–76.
7 Gehrig PA, Bae-Jump VL, Boggess JF, Groben PA, Fowler WC Jr, Van Le L. Association between uterine serous carcinoma and breast cancer. *Gynecol Oncol* 2004; **94**: 208–11.
8 Hinkula M, Pukkala E, Kyyronen P, Kauppila A. Grand multiparity and incidence of endometrial cancer: a population-based study in Finland. *Int J Cancer* 2002; **98**: 912–15.
9 Chubak J, Tworoger SS, Yasui Y, Ulrich CM, Stanczyk FZ, McTiernan A. Associations between reproductive and menstrual factors and postmenopausal sex hormone concentrations. *Cancer Epidemiol Biomarkers Prev* 2004; **13**: 1296–301.
10 Langer RD, Pierce JJ, O'Hanlan KA *et al.* Transvaginal ultrasonography compared with endometrial biopsy for the detection of endometrial disease. Postmenopausal Estrogen/Progestin Interventions Trial. *N Engl J Med* 1997; **337**: 1792–8.
11 Petricoin EF, Liotta LA. SELDI-TOF-based serum proteomic pattern diagnostics for early detection of cancer. *Curr Opin Biotechnol* 2004; **15**: 24–30.
12 Mehta AI, Ross S, Lowenthal MS *et al.* Biomarker amplification by serum carrier protein binding. *Dis Markers* 2003; **19**: 1–10.
13 Hortin GL. The MALDI-TOF mass spectrometric view of the plasma proteome and peptidome. *Clin Chem* 2006; **52**: 1223–37.
14 Lowenthal MS, Mehta AI, Frogale K *et al.* Analysis of albumin-associated peptides and proteins from ovarian cancer patients. *Clin Chem* 2005; **51**: 1933–45.
15 Issaq HJ, Conrads TP, Prieto DA, Tirumalai R, Veenstra TD. SELDI-TOF MS for diagnostic proteomics. *Anal Chem* 2003; **75**: 148A–55A.
16 Chapman K. The ProteinChip biomarker system from ciphergen biosystems: a novel proteomics platform for rapid biomarker discovery and validation. *Biochem Soc Trans* 2002; **30**: 82–7.
17 von Eggeling F, Junker K, Fiedle W *et al.* Mass spectrometry meets chip technology: a new proteomic tool in cancer research? *Electrophoresis* 2001; **22**: 2898–902.
18 Japan Society of Obstetrics and Gynecology, Japanese Society of Pathology, Japan Radiological Society. *The General Rules for Clinical and Pathological Management of Uterine Corpus Cancer*, 2nd edn. Tokyo: Kanahara Shuppan, 1996.
19 Honda K, Hayashida Y, Umaki T *et al.* Possible detection of pancreatic cancer by plasma protein profiling. *Cancer Res* 2005; **65**: 10 613–22.
20 Hayashida Y, Honda K, Osaka Y *et al.* Possible prediction of chemoradiosensitivity of esophageal cancer by serum protein profiling. *Clin Cancer Res* 2005; **11**: 8042–7.
21 Metz CE. Basic principles of ROC analysis. *Semin Nucl Med* 1978; **8**: 283–98.
22 Niloff JM, Klug TL, Schaetzl E, Zurawski VR Jr, Knapp RC, Bast RC Jr. Elevation of serum CA125 in carcinomas of the fallopian tube, endometrium, and endocervix. *Am J Obstet Gynecol* 1984; **148**: 1057–8.
23 Kukura V, Zaninovic I, Hrdina B. Concentrations of CA-125 tumor marker in endometrial carcinoma. *Gynecol Oncol* 1990; **37**: 388–9.
24 Bast RC Jr, Klug TL, St John E *et al.* A radioimmunoassay using a monoclonal antibody to monitor the course of epithelial ovarian cancer. *N Engl J Med* 1983; **309**: 883–7.

doi: 10.1111/j.1349-7006.2007.00458.x

25 Duk JM, Aalders JG, Fleuren GJ, de Bruijn HW. CA 125: a useful marker in endometrial carcinoma. *Am J Obstet Gynecol* 1986; **155**: 1097–102.
26 States DJ, Omenn GS, Blackwell TW *et al.* Challenges in deriving high-confidence protein identifications from data gathered by a HUPO plasma proteome collaborative study. *Nat Biotechnol* 2006; **24**: 333–8.
27 Statistics and Information Department, Minister's Secretariat, Ministry of Health and Welfare, Japan. *Report on the Health Services for the Elderly*. Tokyo: Health and Welfare Statistics Association, 1997.
28 Nakagawa-Okamura C, Sato S, Tsuji I *et al.* Effectiveness of mass screening for endometrial cancer. *Acta Cytol* 2002; **46**: 277–83.

Supplementary Material

The following supplementary material is available for this article:

Fig. S1. Purification of serum-albumin-associated peptides.

Fig. S2. Distribution of the intensity of the 4769-, 6254- and 11 792 m/z-peaks of controls (C) and stage 0 to IV endometrial cancer patients. Solid lines represent the average intensity values of the healthy controls + 2 SD. The broken lines indicate the average intensity in the controls and cancer patients.

This material is available as part of the online article from:

http://www.blackwell-synergy.com/doi/cas/10.1111/j.1349-7006.2007.00458.x

<http://www.blackwell-synergy.com/doi/cas/10.1111/j.1349-7006.2007.00458.x>

(This link will take you to the article abstract).

Please note: Blackwell Publishing are not responsible for the content or functionality of any supplementary materials supplied by the authors. Any queries (other than missing material) should be directed to the corresponding author for the article.

Original Paper

Cells Tissues Organs

Cells Tissues Organs 2007;186:204–209
DOI: 10.1159/000105675

Accepted after revision: May 4, 2007
Published online: July 12, 2007

Sequential Histopathology of Pancreatic Tissues in *aly/aly* Mice

Yoichi Nakamura[a, d] Shuang-Qin Yi[a] Hayato Terayama[a] Munekazu Naito[a]
Jun Li[a] Hiroshi Moriyama[a, c] Akihiko Tsuchida[b] Masahiro Itoh[a]

Departments of [a]Anatomy and [b]Surgery, Tokyo Medical University, and [c]Department of Anatomy, Showa University School of Medicine, Tokyo, and [d]School of Nursing and Rehabilitation Sciences, International University of Health and Welfare, Kanagawa, Japan

Key Words
Alymphoplasia · Pancreatitis · Exocrine gland

Abstract
C57BL/6J strain mice carrying the homozygous autosomal recessive mutation alymphoplasia *(aly)* lack peripheral lymph nodes and Peyer's patches and exhibit chronic infiltration of lymphocytes into various organs. Pancreatitis, one of the inflammatory lesions, is considered to be of autoimmune origin; however, the target autoantigens have not yet been determined. In this study, pancreatic tissues of male *aly/aly* mice and wild-type mice at 1–65 weeks of age were light- and electron-microscopically examined to investigate when and how pancreatitis develops. The results showed that macrophages had first appeared and remained in the lymphatic lumen at 3 weeks of age and then a lot of eosinophilic granulocytes infiltrated into the interlobular connective tissues at 5 weeks of age. After the subsidence of eosinophilic inflammation, macrophages and B220+ cells appeared at the perivascular tissues at 9 weeks of age. Thereafter, both CD4+ and CD8+ cells finally participated in the interstitial inflammation from 11 weeks of age. It was noted that these leukocytes had infiltrated into the perivascular interstitium rather than the parenchymal tissues during the course of pancreatitis, although a large parenchymal area was finally degenerated and replaced by adipose tissue.

Introduction

The C57BL/6$^{aly/aly}$ *(aly/aly)* mouse is a spontaneous mutation of the C57BL/6J strain that lacks both peripheral lymph nodes and Peyer's patches (= congenital alymphoplasia), and shows defects in both humoral and cellular immunity [Miyawaki et al., 1994; Tsubata et al., 1996; Shi et al., 2004]. Previous histopathological analyses of this mouse already revealed that lymphocytic inflammation in various organs such as liver, lungs, salivary glands, lacrimal glands, and pancreas had insidiously occurred around 14 weeks of age and gradually increased in severity as they aged [Furukawa et al., 1996; Tsubata et al., 1996; Komiyama et al., 2001]. However, to our knowledge, histological observation of pancreatitis in *aly/aly* mice has been quite limited so far and there have been no studies on the chronological changes from the inductive to the end stage. Therefore, we sequentially observed the lesions in the present study.

Abbreviations used in this paper

DAB	3,3′-diaminobenzidine tetrahydrochloride
HE	hematoxylin and eosin
PBS	phosphate-buffered saline

KARGER
Fax +41 61 306 12 34
E-Mail karger@karger.ch
www.karger.com

1422–6405/07/1863–0204$23.50/0

Accessible online at:
www.karger.com/cto

Dr. Shuang-Qin Yi
Department of Anatomy, Tokyo Medical University
6-1-1 Shinjuku, Shinjuku-ku
Tokyo 160-8402 (Japan)
Tel. +81 3 3351 6141, ext. 231, Fax +81 3 3341 1137, E-Mail yixim@tokyo-med.ac.jp

Materials and Methods

Animals

Male *aly/aly* and female *aly/+* mice (8 weeks old) were purchased from Nihon Clea (Japan) and mated under pathogen-free conditions. Homozygous *aly/aly* mice were confirmed by checking whether or not there were any mesenteric lymph nodes. Homozygous male *aly/aly* mice (n = 36) and wild-type C57BL/6J mice (n = 9) were sacrificed at 1, 3, 5, 9, 11, 25, 32, 50 and 65 weeks of age. All mice were treated in accordance with the Guide for Animal Experimentation of Tokyo Medical University.

Light- and Electron-Microscopic Observations

Both *aly/aly* mice and wild-type mice were anesthetized with ether, and then their pancreases were removed, fixed in Bouin's solution, dehydrated in an ethanol series and embedded in plastic (Technovit 7100; Kulzer, Germany). Serial plastic transverse sections of 5 μm were cut with a microtome (HN340E, Microtome, Germany), stained with hematoxylin and eosin (HE), and then observed under a light microscope (Olympus, Tokyo, Japan).

For electron microscopy, *aly/aly* mice were anesthetized with ether and then perfused intracardially with saline and thereafter with 2.5% glutaraldehyde in 0.1 M phosphate buffer (pH 7.4). Samples of the pancreas were taken, cut into small pieces, fixed in 2.5% glutaraldehyde [0.1 M phosphate-buffered saline (PBS)], and then postfixed in 1% OsO_4 for 2 h. They were then dehydrated in an ethanol series, substituted with QY-2 (Nissin EM, Japan), and then embedded in epoxy resin (Quetol 651; Nissin EM, Japan). Semithin sections (1.5 μm) were cut, stained with 1% toluidine blue, and observed under a light microscope. The blocks were then retrimmed, and ultrathin sections were cut with a diamond knife. The sections were stained with uranyl acetate and lead citrate, and examined under an electron microscope (H-7000, Hitachi, Japan).

Immunohistochemical Analysis

Aly/aly mice were anesthetized with ether, and then their pancreases were removed. The pancreases were embedded in OCT compound (Tissue-Tek., Mile, Elkhart, Ind., USA), and quickly frozen in liquid nitrogen. Frozen sections (6 μm) were fixed with acetone for 10 min at 4°C and then processed for immunostaining. Immunocytochemical procedures were performed according to our previous papers [Itoh et al., 1999a, b]. Briefly, the sections were immersed for 10 min in Block Ace (Dainippon Pharmaceutical Co., Japan) to block endogenous peroxidase activity, and then washed 3 times in PBS before being preincubated for 20 min in 1.5% normal rabbit serum in PBS to reduce nonspecific staining, and finally washed 3 times in PBS. The sections were incubated with the primary antibodies for 2 h at room temperature and then with the secondary antibodies for 30 min at room temperature. Subsequently the streptavidin-biotinylated peroxidase complex technique (VECTASTAIN Elite ABC Reagent) was used incubating sections with ABC complexes for 30 min at room temperature, and then the sections were fixed in 1% glutaraldehyde in PBS. Immunoreactivity was visualized using 0.02% 3,3′-diaminobenzidine tetrahydrochloride (DAB) for 2–5 min. The sections were counterstained with methyl green and then examined under a light microscope (Olympus, Tokyo, Japan). The primary antibodies were purified rat anti-mouse CD4 (1:50, monoclonal, class II MHC-restricted T cell marker, including most T helper cells, Cat. No. 550278, BD Pharmingen, USA), purified rat anti-mouse CD8 (1:50, monoclonal, class I MHC-restricted T cell marker, including most T suppressor/cytotoxic cells, Cat. No. 550281, BD Pharmingen, USA), rat anti-mouse CD45R/B220 (B220, 1:50, monoclonal, markers of B cells and some activated T cells, Cat. No. 550286, BD Pharmingen, USA), and rat anti-mouse F4/80 (1:100, monoclonal, macrophage marker, Cat. No. ab6640, Abcam, UK) antibodies. The secondary antibody was biotinylated rabbit anti-rat IgG (VECTASTAIN Elite ABC kit, Vector Lab, USA). Control sections not treated with the primary monoclonal antibodies were prepared at the same time.

Results

The histological appearance of the pancreases in *aly/aly* mice at 1 week of age showed no inflammatory cell responses as in the wild-type control mice (fig. 1a). However, differing from control mice, at 3 weeks of age in *aly/aly* mice, many macrophages appeared and remained in the lumina of the lymphatic vessels (fig. 1b). Furthermore, at 5 weeks of age in *aly/aly* mice, a lot of eosinophilic granulocytes infiltrated into the interlobular connective tissues around the vascular and lymphatic vessels before the induction of lymphocytic inflammation (fig. 1c, d).

In 9-week-old mice, eosinophilic inflammation disappeared, and B220+ cells and F4/80+ cells infiltrated into perivascular regions (fig. 2). However, CD4+ and CD8+ cells were hardly seen at this age. In 11-week-old mice,

(For figure see next page.)

Fig. 1. a A toluidine blue-stained semithin section of a pancreas of an *aly/aly* mouse at 1 week of age. No lesion was found. **b** A toluidine blue-stained semithin section of a pancreas of an *aly/aly* mouse at 3 weeks of age. Monocytes/macrophages (arrow) were packed in the lymphatic vessels. **c** An HE-stained section of a pancreas of a 5-week-old *aly/aly* mouse. A lot of leukocytes (asterisk) have infiltrated into the interlobular connective tissues. **d** An HE-stained section at a highly magnified view of the same mouse as in **c**. The infiltrating leukocytes were found to be eosinophilic granulocytes. **e** A toluidine blue-stained semithin section of a pancreas of an 11-week-old *aly/aly* mouse. A lymphatic lumen was occupied by a big lump of cells (asterisk). **f** An electron micrograph of the region around the asterisk of **e**. Many lymphocytes and macrophages were packed. **g** An HE-stained section of a pancreas of a 32-week-old *aly/aly* mouse. **h** A highly magnified view of box h in **g**. Infiltration of lymphocytes (arrow) and degeneration of the exocrine tissue can be seen. **i** An HE-stained section of a pancreas of a 50-week-old *aly/aly* mouse. The exocrine parenchyma was extensively degenerated and replaced by adipose tissue (asterisks). **j** A highly magnified view of

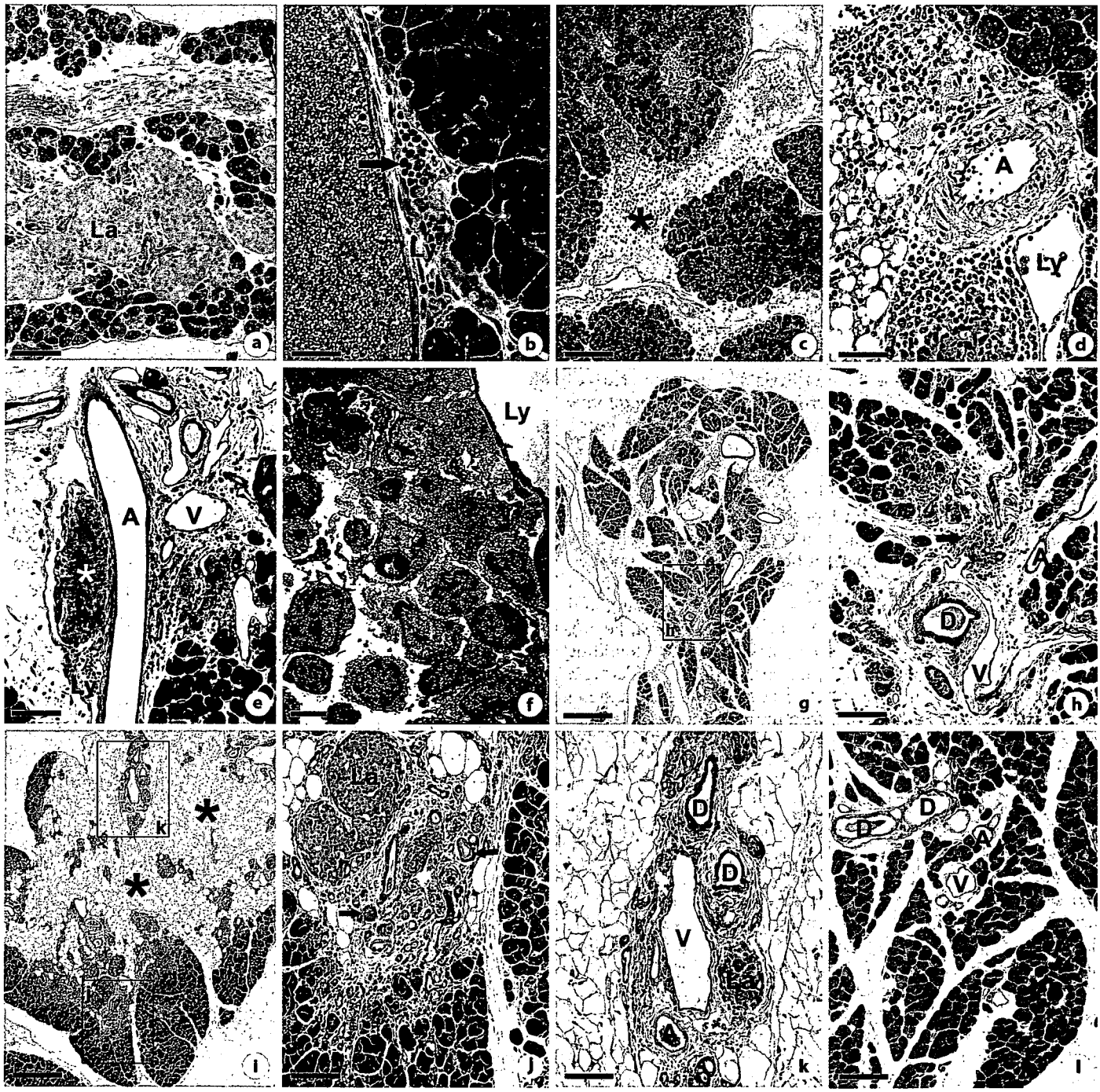

box j in **i**. Proliferation of some pancreatic ducts was observed (arrows) among the lymphocytic infiltration. **k** A highly magnified view of box k in **i**. An islet of Langerhans remained in spite of extensive degeneration of the exocrine tissue. **l** An HE-stained section of a pancreas of a 16-week-old C57BL/6J mouse. No inflammation and degeneration were found. A = Artery; D = pancreatic duct; La = islet of Langerhans; Ly = lymph vessel; V = vein. Scale bars: 100 μm (**a**, **h**, **j**, **k**, **l**); 200 μm (**c**, **e**); 50 μm (**b**, **d**); 10 μm (**f**); 500 μm (**g**, **i**).

Fig. 2. Immunohistochemical localization of CD4+, CD8+, B220+, or F4/80+ positive cells in the pancreases of 9, 11, 25 and 50-week-old *aly/aly* mice. In a 9-week-old mouse, B220+ and F4/80+ cells could be seen in the perivascular regions of the pancreas. Infiltration of CD4+ cells in the pancreas became conspicuous at 11 weeks of age. Then CD8+ cells also appeared around the blood and lymph vessels in a 25-week-old mouse. At 50 weeks of age, CD4+ cells mainly infiltrated into the perivascular tissues. A = Artery; D = pancreatic duct; V = vein. Scale bars: 100 μm.

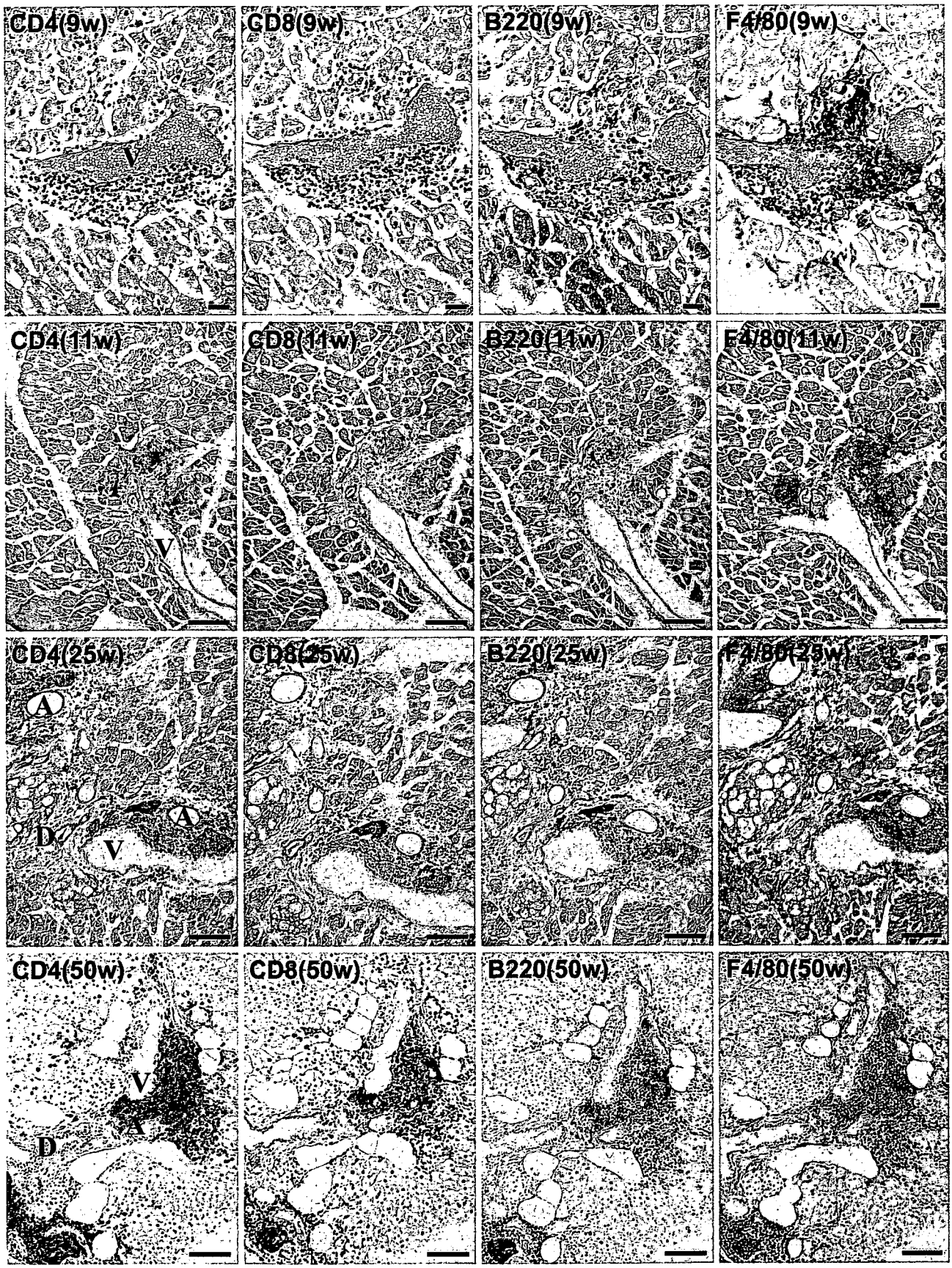
CD4(9w)
CD8(9w)
B220(9w)
F4/80(9w)
V
CD4(11w)
CD8(11w)
B220(11w)
F4/80(11w)
A
V
CD4(25w)
CD8(25w)
B220(25w)
F4/80(25w)
A
D
A
V
CD4(50w)
CD8(50w)
B220(50w)
F4/80(50w)
V
A
D

2

CD4+ cells significantly started to infiltrate around the blood vessels in the interlobular connective tissues with many F4/80 cells (fig. 2). In lymphatics of 11-week-old mice, the presence of some lumps of mononuclear cells was specifically noted (fig. 1e), and the electron-microscopic observation revealed that these lumps were composed of densely packed lymphocytes and macrophages (fig. 1f). In 25-week-old mice, CD8+ cells had also become conspicuous around the blood vessels and lymphatics (fig. 2).

In 32-week-old mice, a few lymphocytes had focally infiltrated from the perivascular tissues into the exocrine parenchyma, and the acinar cells adjacent to the infiltrating lymphocytes were undergoing focal degeneration (fig. 1g, h). In 50-week-old mice, the exocrine parenchyma was extensively destroyed, being replaced by adipose tissue (fig. 1i). However, the direct infiltration of lymphocytes into the exocrine parenchymal tissues was still limited and most leukocytes involving CD4+ cells, CD8+ cells, B220+ cells and F4/80+ cells had remained in the interlobular connective tissues (fig. 2). It was also noted that some islets of Langerhans had remained and some pancreatic ducts had newly regenerated in the area of lymphocytic inflammation and severe parenchymal degeneration (fig. 1j, k). In contrast, the pancreases of all examined wild-type control mice of 1–65 weeks of age had parenchymal tissue of normal appearance and were free from inflammatory cell infiltration and parenchymal degeneration (fig. 1l).

Discussion

In the present study, the sequential histological changes of the pancreas in *aly/aly* mice were examined. Although inflammatory lesions had been reported to develop insidiously around 14 weeks of age [Tsubata et al., 1996], our results showed that many macrophages had packed in the pancreatic lymphatic lumina at 3 weeks of age and then a lot of eosinophilic granulocytes had infiltrated into the interlobular connective tissues at 5 weeks of age. Furthermore, many F4/80+ and some B220+ cells infiltrated into the connective tissues at 9 weeks of age before infiltration of T cells. Therefore, the present study first demonstrated that the pancreatic pathological signs of *aly/aly* mice start as early as 3 weeks of age. Although it remains unclear why the infiltration of macrophages and eosinophils preceded the lymphocytic inflammation, we previously observed that a lot of macrophages and eosinophils but not lymphocytes infiltrated into the epididymides and vasa deferentia of *aly/aly* mice of 10 weeks of age [Itoh et al., 1999a]. Therefore, abnormal infiltration of not only lymphocytes but also macrophages and eosinophils should be a characteristic feature of *aly/aly* mice.

Tsubata et al. [1996] reported that most infiltrated cells in the pancreas were CD4+ T cells in 24-week-old *aly/aly* mice. They also demonstrated that pancreatitis can be transferred to recipient mice by CD4+ spleen cells of *aly/aly* mice. These results indicate that CD4+ T cell-mediated immune responses against the pancreatic autoantigens are responsible for the spontaneous pancreatitis in *aly/aly* mice [Okazaki et al., 2001]. However, we observed here that macrophages, eosinophilic granulocytes, and B220+ cells had appeared in the perivascular regions before accumulation of CD4+ T cells. Moreover, CD8+ T cells also participated later in the pancreatic inflammation. Therefore, it was found that various populations of leukocytes are involved in the inflammation in *aly/aly* mice. There remains a possibility that B220+ cells detected in the pancreatic lesions were of activated T cells but not B cells. However, B220+ but CD4– and CD8– cells were detected at 9 weeks of age. This indicates that B220+ cells in the pancreas are B cells, although autoantibodies against the pancreatic cells have not yet been identified [Tsubata et al., 1996; Okazaki et al., 2001; Okazaki and Chiba, 2002]. Additionally, we noticed scattered mononuclear cells that had not been immunostained among F4/80+ cells and B220+ cells in early pancreatic lesions. Populations of these scattered mononuclear cells were not identified in the present study. They might be primitive T cells such as natural killer cells and large granular lymphocytes because of a deficiency of mature T and B cells in *aly/aly* mice [Konishi et al., 2000; Coles et al., 2006]. Moreover, it was also notable that the regeneration of some pancreatic ducts was observed in areas of the lymphocytic infiltration and the exocrine degeneration. This feature is also induced in pancreas after the duct ligature [Watanabe et al., 1995; Hamamoto et al., 2002]. It may be that the inflammatory cells attacked the inter- and intralobular ducts and then occluded the pancreatic ducts, resulting in spreading degeneration and local regeneration of the pancreatic acini. Furthermore, direct infiltration of lymphocytes into the pancreatic acini was very limited even in fully developed pancreatitis. This also implies that focal occlusion of the pancreatic ducts rather than autoimmune damage against each pancreatic acinus might be involved in the widespread parenchymal degeneration. Furthermore, our observation suggests that damage to pancreatic acini rather than Langerhans

islets is a characteristic histopathology of pancreatitis. To investigate the complicated and age-dependent sequences underlying the pancreatic inflammation and degeneration more minutely, quantitative and topographical analyses of leukocyte subsets and various cytokines from 3 weeks of age will be planned in the next study.

Acknowledgements

We are grateful to Ms Miyuki Kitaoka, Ms Fumiko Komoda, and Ms Yuki Ogawa for their excellent technical assistance during this study.

References

Coles, M.C., H. Veiga-Fernandes, K.E. Foster, T. Norton, S.N. Pagakis, B. Seddon, D. Kioussis (2006) Role of T and NK cells and IL7/IL7r interactions during neonatal maturation of lymph nodes. Proc Natl Acad Sci USA *103:* 13457–13462.

Furukawa, M., A. Sakamoto, Y. Kita, Y. Ohishi, R. Matsumura, R. Tsubata, T. Tsubata, I. Iwamoto, Y. Saito, T. Sumida (1996) T-cell receptor repertoire of infiltrating T cells in lachrymal glands, salivary glands and kidneys from alymphoplasia (aly) mutant mice: a new model for Sjögren's syndrome. Br J Rheumatol *35:* 1223–1230.

Hamamoto, N., N. Ashizawa, M. Niigaki, T. Kaji, T. Katsube, H. Endoh, M. Watanabe, S. Sumi, Y. Kinoshita (2002) Morphological changes in the rat exocrine pancreas after pancreatic duct ligation. Histol Histopathol *17:* 1033–1041.

Itoh, M., K. Miyamoto, T. Ooga, K. Iwahashi, Y. Takeuchi (1999a) Spontaneous accumulation of eosinophils and macrophages throughout the stroma of the epididymis and vas deferens in alymphoplasia (aly) mutant mice. I. A histological study. Am J Reprod Immunol *42:* 246–253.

Itoh, M., Q. Xie, K. Miyamoto, Y. Takeuchi (1999b) F4/80-positive cells rapidly accumulate around tubuli recti and rete testis between 3 and 4 weeks of age in the mouse: an immunohistochemical study. Am J Reprod Immunol *42:* 321–326.

Komiyama, K., J. Sato, M. Okaue, T. Goto, S. Horimoto, T. Akagi, S. Akima, I. Moro (2001) Histopathological and immunohistological analyses in IgA deficient lymphoplasia *(aly/aly)* mouse. J Oral Sci *43:* 91–96.

Konishi, J., K. Iwabuchi, C. Iwabuchi, M. Ato, J. I. Nagata, K. Onoe, K.I. Nakagawa, M. Kasai, K. Ogasawara, K. Kawakami, K. Onoe (2000) Thymic epithelial cells responsible for impaired generation of NK-T thymocytes in Alymphoplasia mutant mice. Cell Immunol *206:* 26–35.

Miyawaki, S., Y. Nakamura, H. Suzuka, M. Kobe, R. Yasumizu, S. Ikehara, Y. Shibata (1994) A new mutation, aly, that induces a generalized lack of lymph nodes accompanied by immunodeficiency in mice. Eur J Immunol *24:* 429–434.

Okazaki, K., T. Chiba (2002) Autoimmune-related pancreatitis. Gut *51:* 1–4.

Okazaki, K., K. Uchida, T. Chiba (2001) Recent concept of autoimmune-related pancreatitis. J Gastroenterol *36:* 293–302.

Shi, M., B. Xu, X. Wang, K. Aoyama, S.A. Michie, T. Takeuchi (2004) Oxidative damages in chronic inflammation of a mouse autoimmune disease model. Immunol Lett *95:* 233–236.

Tsubata, R., T. Tsubata, H. Hiai, R. Shinkura, R. Matsumura, T. Sumida, S. Miyawaki, H. Ishida, S. Kumagai, K. Nakao, T. Honjo (1996) Autoimmune disease of exocrine organs in immunodeficient alymphoplasia mice: a spontaneous model for Sjögren's syndrome. Eur J Immunol *26:* 2742–2748.

Watanabe, S., K. Abe, Y. Anbo, H. Katoh (1995) Changes in the mouse exocrine pancreas after pancreatic duct ligation: a qualitative and quantitative histological study. Arch Histol Cytol *58:* 365–374.

Usefulness of serum protein profiling for prediction of preoperative chemoradiosensitivity of esophageal cancer

YOSHIHIRO OTA[1], YU TAKAGI[1], YOSHIAKI OSAKA[1], MOTOO SHINOHARA[1], SUMITO HOSHINO[1], AKIHIKO TSUCHIDA[1], TATSUYA AOKI[1], KAZUFUMI HONDA[2] and TESSHI YAMADA[2]

[1]Third Department of Surgery, Tokyo Medical University; [2]Chemotherapy Division and Cancer Proteomics Project, National Cancer Center Research Institute, Tokyo 160-0023, Japan

Received March 2, 2007; Accepted May 23, 2007

Abstract. We examined whether serum protein profiling is a reliable index for prediction of therapeutic efficacy of preoperative chemoradiotherapy (PCRT) in advanced esophageal cancer compared with evaluation of the efficacy of conventional clinical examination. We entered 42 patients who received PCRT and surgery between 1998 and 2002 into this study. Serum protein profiling was performed using the preoperative serum of the patient to select the marker set that enabled the efficacy of PCRT to be evaluated accurately. The efficacy of PCRT was predicted with the marker set, and the sensitivity, specificity and accuracy of the method were calculated based on evaluation of the efficacy by pathological examination. Similarly, therapeutic efficacy was also predicted based on evaluation of the efficacy of conventional clinical examination, and the results were compared with those of prediction by serum protein profiling. The correlation between each predictive examination and outcome was evaluated. The sensitivity, specificity and accuracy of prediction of therapeutic efficacy of PCRT by serum protein profiling were 90.9, 100 and 93.3%, respectively. In clinical examination, prediction of the efficacy of PCRT by three methods was as follows: by esophagography, sensitivity 76.0%, specificity 17.6%, accuracy 52.4%; by endoscopy, sensitivity 80.0%, specificity 11.8%, accuracy 52.4%; by computed tomography, sensitivity 60.0%, specificity 47.1%, accuracy 54.8%, respectively. These results demonstrated the superiority of serum protein profiling in predicting the therapeutic efficacy of PCRT compared with conventional clinical examination. Moreover, serum protein profiling was the only significant prognostic factor as regards the correlation with outcome by multivariate analysis.

Correspondence to: Dr Akihiko Tsuchida, Third Department of Surgery, Tokyo Medical University, 6-7-1 Nishi-Shinjuku, Shinjuku-ku, Tokyo 160-0023, Japan
E-mail: akibobo@hotmail.com

Key words: esophageal cancer, chemoradiotherapy, serum protein profiling, proteomics

Introduction

Esophageal cancer generally has a poor prognosis and cannot be cured by surgery alone because it readily develops lymph node metastasis or invades into the trachea, bronchi or large vessels, especially if advanced. Since esophageal cancer is sensitive to chemotherapy and radiotherapy, various approaches to multidisciplinary treatment in which chemoradiotherapy is combined with surgical treatment have been made. Among them, preoperative chemoradiotherapy (PCRT), which came into use in the 1980s in Europe and North America, is reported to enhance the treatment results of advanced esophageal cancer by improving resection rates evaluating local control or by inhibiting post-operative recurrence by controlling minute metastatic lesions (1-3). However, several studies have revealed that PCRT does not affect all patients with esophageal cancer but improves the survival rates only when it is pathologically effective (4,5). In ineffective cases, PCRT is actually disadvantageous due to its side effects. It is therefore important to properly predict the therapeutic efficacy of PCRT and to use PCRT only for those cases in which effect can be anticipated. In order to discover a new diagnostic that can accurately predict the efficacy of PCRT, we performed serum protein profiling using preoperative serum of the patient and reported that efficacy could be accurately predicted (6).

In the present study, we compared the evaluation of efficacy of conventional clinical examination as regards the accuracy of prediction and correlation with outcome, and objectively assessed the prediction of therapeutic efficacy of PCRT by serum protein profiling to gain insight into the usefulness of PCRT.

Patients and methods

Patients. Forty-two patients with esophageal squamous cancer that underwent PCRT and surgery at the Third Department of Surgery, Tokyo Medical University Hospital between January 1998 and December 2002 were enrolled in the study. The characteristics of the patients were as follows: mean age, 61.7; gender, 37 men and 5 women; tumor location, 2 in cervical area; 7 in the upper thoracic area; 21 in the middle thoracic area; 11 in the lower thoracic area; and 1

Table I. Patient characteristics.

No. of patients	42
Male/female	37/5
Age (years, mean ± SD)	61.7±6.9
Tumor location	
Ce	2
Ut	7
Mt	21
Lt	11
Ae	1
Clinical stage	
II	7
III	29
IV	6

Ce, cervical esophagus; Ut, upper thoracic esophagus; Mt, middle thoracic esophagus; Lt, lower thoracic esophagus; Ae, abdominal esophagus.

in abdomen; clinical stage, 7 in stage II; 29 in stage III; and 6 in stage IV (Table I).

Preoperative chemoradiotherapy (PCRT). In PCRT, low dose FP (CDDP 10 mg/m^2/day, 5 days a week for 2 weeks, total 100 mg/m^2 + 5-FU 350 mg/m^2/day, 5 days a week for 4 weeks, total 7,000 mg/m^2) and radiation (10-MV linear accelerator 2 Gy/day, 5 days a week for 4 weeks, total 40 Gy) were administered concurrently. The radiation field was set to include both the primary lesion and accessory lymph nodes. Approximately 2 weeks after PCRT, the effects on the primary lesion and accessory lymph nodes were assessed by esophagography, esophagoscopy, computed tomography (CT) and endoscopic ultrasonography. The operation was performed ~4 weeks after PCRT. The esophagus was resected via a right thoracotomy, and 3-field lymphadenectomy was performed in the cervical, thoracic and abdominal regions.

Radiological and pathological criteria for the effects of PCRT. The criteria for radiological response in the primary lesion were defined by the Japanese Society for Esophageal Disease (7). Complete response (CR), the disappearance of tumor shadow on esophagography plus disappearance of the tumor and a flat mucosal surface on esophagography; partial response (PR), a reduction rate [RR = (pretreatment tumor volume)-(post-treatment tumor volume)/(pretreatment tumor volume x 100%)] of 50% or more, on esophagography, there is a marked reduction in tumor shadow, and on esophagography, there is a flattening of tumor or reduction of protrusions at the periphery of the ulcer, plus decreased depth of the ulcer; no change (NC), RR is <50% or increases by up to 25%, on esophagography, there is either no change or a slight reduction of the tumor and no change or flattening of the protrusion at the ulcer periphery; progressive disease (PD), RR increases 25% or more, on esophagography, there is an increase of the tumor shadow or the appearance of a new lesion. In evaluating the therapeutic efficacy of PCRT, CR and PR were evaluated as effective and NC and PD as ineffective.

Pathological response criteria were defined as follows: grade 0, no discernible therapeutic effect on cancer tissue or cells; grade 1, apparently viable cells account for 1/3 or more of tumor tissue, but there is some evidence of degeneration of cancer tissue or cells; grade 2, viable cancer cells account for <1/3 of tumor tissue, while other cancer cells are severely degenerated or necrotic; grade 3, no viable cancer cells evident. Grades 0 and 1 were evaluated as ineffective and grades 2 and 3 as effective.

Surface-enhanced laser desorption and ionization coupled with hybrid quadrupole time-of-flight mass spectrometry (SELDI-TOF-MS) analysis. To denature serum proteins, 90 μl of U9 buffer {9 mol/l urea, 2% 3-[(3-cholamidopropyl) dimethylammonio]-1-propanesulfonic acid, and 50 mmol/l Tris-HCl (pH 9)} was added to 10 μl of each sample and vortexed for 20 min. To increase the number of detectable protein peaks, we used 4 different ProteinChip (Ciphergen Biosystems, Inc., Fremont, CA, USA) array/wash conditions, i.e., reversed phase (H50), weak cation exchanger with low stringent wash (CM10/pH 4.0), cation exchanger with high stringent wash (CM10/pH 7.0) and immobilized metal affinity capture coupled with copper (IMAC-Cu^{2+}), as instructed by the supplier. Each sample was randomly assigned in duplicate to one of 96 spots of 12 allied ProteinChip arrays with a Biomek 2000 laboratory workstation (Beckman Coulter Inc., Fullerton, CA, USA). Sinapinic acid solution was prepared in 50% v/v acetonitrile and 5% v/v trifluoroacetic acid as an energy-absorbing matrix, and 1 μl of saturated solution was applied to each spot on the chips. Low-molecular-weight proteins in the 2,000-40,000 m/z range were read on a high-resolution performance hybrid quadrupole time-of-flight mass spectrometer Q-star XL (Applied Biosystems, Foster City, CA) equipped with a PCI 1000 ion source (Ciphergen). The laser intensity, frequency, and accumulation time of the instrument were set at 60%, 25 Hz, and 90 sec, respectively. Mass accuracy was externally calibrated on the day of the measurements by using the all-in-one-peptide molecular mass standard (Ciphergen).

Peak detection and quantification. The mass data were converted to text files consisting of m/z and intensity after mass calibration by Analyst QS (Applied Biosystems) and processed by the following procedures. First, the spectrum was smoothed with a Gaussian window function (weighting addition by the following function). Baseline and noise level were calculated by making the bottom 10 percentile in descending order and 2 x (10-5% point), respectively, for every 200 m/z interval, which divided the range of 2,000-40,000 m/z, and by connecting each section by natural spline interpolation (8). Maximum intensity was calculated for every 1 m/z interval. All apices and valleys of the intensity arrangement were detected first. The depths of adjoining low peaks and valleys were then calculated, and if the depth was <4 signal-to-noise ratios (S/N), it was merged into higher peaks. Peak alignment was performed so that the number of samples with a >8 S/N peak in the tolerance level of m/z 0.05% would become the maximum. If a sample had a >16 S/N peak or the proportion

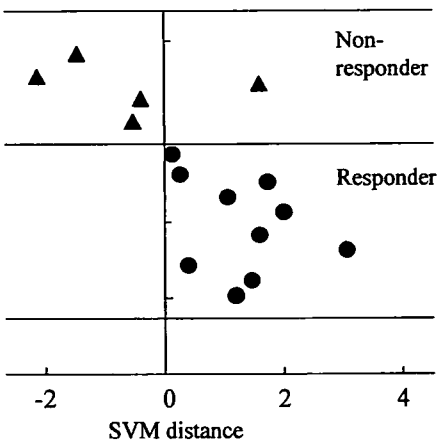

Figure 1. Results of serum protein profiling in the validation set (n=15). Sensitivity is 90.9% (10/11), specificity is 100% (4/4) and accuracy is 93.3% (14/15).

of samples with a >4 S/N peak was >40%, the peaks were used for marker discovery. Finally, peak intensity was normalized so that the total intensity after baseline subtraction would be the same for all samples in the 2,000-40,000 m/z range. Peak images were generated with Analyst QS and MassNavigator software (Mitsui Knowledge Industry, Tokyo, Japan).

SELDI-TOF-MS was used to perform serum protein profiling. Serum of a total of 27 patients, 15 responders of grade 2 and 3 and 12 non-responders of grade 0 and 1 with no significant difference in age, gender, tumor location and clinical stage, underwent serum protein profiling as a training set, and the profiling pattern that could distinguish responders and non-responders with an accuracy of 100% was identified and a marker set was extracted. Usefulness of the marker set was then examined with a validation set consisting of 15 other cases (10 responders and 5 non-responders).

Evaluation of PCRT and statistical analysis. The therapeutic efficacy of PCRT was examined by evaluating the efficacy of conventional clinical examinations and by serum protein profiling to examine the sensitivity, specificity and accuracy of individual items by comparison with the efficacy of pathological response. In addition, cumulative survival rates of the 42 patients were calculated by the Kaplan-Meier method, and the correlation between outcome and the prediction of the therapeutic efficacy based on evaluation of clinical examination and from serum protein profiling was examined using univariate and multivariate analyses. A p-value of <0.05 was considered to indicate a statistically significant difference.

Results

Predictive efficacy of serum protein profiling. Serum protein profiling was performed on 42 patients with esophageal cancer using SELDI-TOF-MS and a total of 859 peak values (mean correlation coefficient: 0.960±0.019) that reflected serum samples within the range of 2,000-40,000 m/z were selected. From those peak values, the combination of peaks that enabled the best predictive efficacy was sought using the training set of 27 case specimens with the support vector machine (SVM). As a result, the combination of four peaks of 7,420 (H50), 9,112 (H50), 17,123 (CM10/pH 4.0) and 12,876 (IMAC-Cu^{2+}) m/z was found as a biomarker to be able to diagnose the 15 responders with 100% sensitivity and the 12 non-responders with 100% specificity. These biomarkers were then evaluated using a validation set of 15 cases. The result was 90.9% sensitivity (10/11), 100% specificity (4/4) and 93.3% accuracy (14/15), demonstrating that serum protein profiling provided highly accurate prediction of the therapeutic efficacy of PCRT (Fig. 1).

Relationship between the predictive efficacy of conventional clinical examination and pathological response. The predictive efficacies of conventional clinical examination and pathological response were compared. The sensitivity, specificity and accuracy of the efficacy evaluation were as follows respectively: by esophagography, 76.0% (19/25), 17.6% (3/17) and 52.4% (22/42); by endoscopy, 80.0% (20/25), 11.8% (2/17) and 52.4% (22/42); by CT, 60.0% (15/25), 47.1% (8/17) and 54.8% (23/42) (Table II). These figures showed

Table II. Relationship between the predictive efficacy of conventional examination and pathological response in primary lesion.

	Esophagography		Endoscopy		CT	
	CR+PR	NC	CR+PR	NC	CR+PR	NC
Pathological response						
Grade 2 and 3	19	6	20	5	15	10
Grade 0 and 1	14	3	15	2	9	8
Sensitivity (%)	76.0		80.0		60.0	
Specificity (%)	17.6		11.8		47.1	
Accuracy (%)	52.4		52.4		54.8	

CR, complete response; PR, partial response; NC, no change.

Table III. Univariate and multivariate analysis in each predictive efficacy for survival.

Variable	Hazard ratio	Confidence interval		Univariate p-value	Multivariate p-value
		<95%	>95%		
Esophagography	0.851	0.282	2.571	0.7749	0.7028
Endoscopy	1.266	0.419	3.827	0.5150	0.2752
CT	0.738	0.296	1.840	0.6756	0.3435
Proteome	2.896	1.154	7.267	0.0234	0.0144
Pathology	2.522	1.018	6.252	0.0457	0.0254

that prediction by conventional clinical examination is less accurate than by serum protein profiling.

Correlation between each predictive examination and survival. The correlation between each predictive examination method and survival was evaluated by univariate and multivariate analyses. Prediction by serum protein profiling proved to be the only effective prognostic factor, with p=0.0234 on univariate analysis and p=0.0144 on multivariate analysis (Table III). In addition, pathological response was also an effective prognostic factor with p=0.0457 in the univariate analysis and p=0.0254 in the multivariate analysis in agreement with previous reports.

Discussion

We set out to determine whether serum protein profiling is useful for predicting therapeutic efficacy of PRCT. Recent significant technological innovations in mass analysis in basic studies of proteomics have allowed highly sensitive detection of protein from small amounts of samples (9). Research and development have therefore been carried out to find new biomarkers using serum protein profiling. Many groups of patients and control subjects have been prepared as training sets whose age, gender, timing of blood sampling, method of blood sampling and blood preservation method are matched, and various machine learning algorithms (support vector machine) that can be applied to artificial intelligence have been made to study the proteomic patterns of both groups and hence extract patient-specific data sets. Once the data sets are precisely defined, both groups can be accurately distinguished even when validation samples without any clinical information are examined (10). We have so far performed serum protein profiling on preoperative serum of patients with esophageal cancer using SELDI-TOF-MS and reported that both responders and non-responders of PCRT could be predicted accurately (6). In this study, the usefulness of prediction by serum protein profiling was validated by making a comparison with the evaluation of the efficacy of conventional clinical examination by esophagography, endoscopy and CT. These results showed the superiority of serum protein profiling for predicting efficacy in terms of sensitivity, specificity and accuracy compared with conventional clinical examinations. One of the reported reasons for this is a probable inconsistency between evaluation of the efficacy of conventional clinical examinations and pathological response (11). In the present study, 42.4% (14/33), 42.9% (15/35) and 37.5% (9/24) of cases respectively classified as effective on the basis of esophagography, endoscopy and CT were found to be pathologically grade 0 and 1. This indicates an inconsistency between efficacy evaluation by diagnostic imaging and by histopathological examination. This is attributable to at least the following two reasons: i) there are cases in which viable cancer cells remain in large numbers, despite seemingly decreasing tumor volumes on clinical examinations; ii) viable cancer cells are not easily detected in endoscopic biopsy, because resected specimens show that they are mainly scattered from submucosal layers to muscle layers, epidermis of which is usually covered with regenerative epithelia. Shiozaki *et al* reported similar results (12,13). Predicting pathological response from diagnostic imaging alone, such as esophagography, endoscopy or CT, is extremely difficult. Although PCRT is advantageous in significantly effective cases, in ineffective cases one whole month might pass in vain, and the best timing for operation could be lost. It is therefore important to predict the therapeutic efficacy of PCRT before treatment and perform chemoradiation only in those cases in which it is likely to be effective. Our results suggest that serum protein profiling is the most accurate method available today.

Apart from esophagography, endoscopy and CT, endoscopic ultrasonography is reported to be useful for evaluating efficacy for clinical examination (14), although it is not normally used due to problems related to manipulative skills and evaluation criteria. Positron emission tomography (PET) is also reported to be useful, and has been gradually recognized as a less-invasive examination technique that can directly reflect pathological response (15,16), although it has not yet been compared with pathological response because of a lack of general availability due to difficulties of the facilities and cost. Moreover, although it is still at the investigative stage, expression of mutant p53 protein in tumors and chemoradiosensitivity has been reported. Lowe *et al* (17) reported that after chemoradiation was performed on nude mice implanted subcutaneously with embryonic fibroblasts with or without p53 genes, a high proportion of tumors with p53 genes

displayed apoptosis and their development was inhibited. The same report described extensive mutation when exons 5-8 of those tumors with p53 genes that did not respond to the treatment were observed, suggesting that the expression of wild-type p53 protein in a tumor can be a marker for chemoradiosensitivity. On the basis of this report, Ikeguchi *et al* (18) examined the expression of mutant p53 protein and the duration of cancer recurrence on resected specimens of a progressive esophageal cancer case that was categorized as non-curative resection due to residual cancer cells, and reported the potential of the mutant p53 protein expression as a marker for chemoradiosensitivity (19). Unfortunately, the usefulness of the expression of mutant p53 protein as a marker for sensitivity to PCRT has not yet been established. Apart from p53, several studies have reported p21 and other genetic markers and efficacy prediction factors such as CDC25B, VEGF and CD34 (20,21), but clinical applications of these results are limited and not yet established. Most studies on the malignancy of cancer by molecular biological approaches constitute retrospective examinations. If those studies are to be applied to clinical diagnoses, prospective studies must be conducted, but such studies require biopsy specimens and so only materials from part of the tumor surface are used for the evaluation; it is questionable whether such materials represent the whole characteristics of a tumor. All cancer cells in a tumor are rarely stained uniformly when the entire tumor is stained; in most cases stained and non-stained parts coexist, so false positives or false negatives can easily occur when the evaluation is based on immunostaining of biopsy specimens. In contrast, serum protein profiling can obtain virtually the same results regardless of age, gender, tumor location and clinical stage as well as sampling method, sampling volume and other conditions of the tumor.

Pathological response in resected specimens has been shown to correlate with prognosis, and a good prognosis is expected in cases where PCRT is pathologically effective. Serum protein profiling was shown in the present study to be an independent prognostic factor in univariate and multivariate analyses of the correlation with outcome, as pathological response can be accurately predicted by proteomic profiling. All cases shown to be sensitive to PCRT by serum protein profiling can therefore candidate for preoperative treatment (22). Although further studies with more samples are needed for clinical applications, prediction of the therapeutic efficacy of PCRT in esophageal cancer by serum protein profiling using the patient's serum is useful for application of PCRT and prediction of prognosis, promoting patient-specific treatment for individual patients with esophageal cancer.

Acknowledgements

This study was supported by the 'Third-Term Comprehensive Control Research for Cancer' conducted by the Ministry of Health, Labor and Welfare of Japan. The authors are indebted to Professor J. Patrick Barron of the International Medical Communications Center of Tokyo Medical University for his review of this manuscript.

References

1. Le Prise E, Etienne PL, Meunier B, *et al*: A randomized study of chemotherapy, radiation therapy, and surgery versus surgery for localized squamous cell carcinoma of the esophagus. Cancer 73: 1779-1784, 1994.
2. Apinop C, Puttisak P and Preecha N: A prospective study of combined therapy in esophageal cancer. Hepatogastroenterol 41: 391-393, 1994.
3. Bosset JF, Gignoux M, Triboulet JP, *et al*: Chemoradiotherapy followed by surgery compared with surgery alone in squamous-cell cancer of the esophagus. N Engl J Med 337: 161-167, 1997.
4. Osaka Y, Takagi Y, Tsuchida A, *et al*: Concurrent preoperative chemoradiotherapy for stage III or IV esophageal squamous carcinoma. Oncol Rep 12: 1121-1126, 2004.
5. Osaka Y, Takagi Y, Hoshino S, *et al*: Effective of preoperative chemoradiotherapy for advanced esophageal carcinoma. J Jap Coll Surg 29: 6-12, 2004.
6. Hayashida Y, Honda K, Osaka Y, *et al*: Possible prediction of chemoradiosensitivity of esophageal cancer by serum protein profiling. Clin Cancer Res 11: 8042-8047, 2005.
7. The Japanese Society for Esophageal Diseases: Guidelines for the Clinical and Pathologic Studies on Carcinoma of the Esophagus. Isono K (ed). 9th edition. Kanehara Shuppan, Tokyo, 1999.
8. Gras R, Muller M, Gasteiger E, *et al*: Improving protein identification from peptide mass fingerprinting through a parameterized multi-level scoring algorithm and an optimized peak detection. Electrophoresis 20: 3535-3550, 1999.
9. Yamada T: Proteome-based approach to cancer diagnosis and treatment. J Jap Soc Oral Maxillofacial Surg 51: 8-9, 2005.
10. Aoshima K: The proteomics general remarks. Cognition Dementia 3: 217-231, 2004.
11. Doki Y, Kabuto T, Ishikawa O, *et al*: Diagnostic image for neoadjuvant chemoradiation therapies toward advanced esophageal cancers. Surg Treat 84: 454-464, 2001.
12. Shiozaki H and Yano M: Neoadjuvant chemoradiotherapy in patients with surgically treated T4 esophageal squamous cell carcinoma. J Jap Surg Soc 103: 284-289, 2002.
13. Yano M, Inoue M and Shiozaki H: Preoperative concurrent chemotherapy and radiation therapy followed by surgery for esophageal cancer. Ann Thorac Cardiovasc Surg 8: 123-130, 2002.
14. Zuccaro G Jr, Rice TW, Goldblum J, *et al*: Endoscopic ultrasound cannot determine suitability for esophagectomy after aggressive chemoradiotherapy for esophageal cancer. Am J Gastroenterol 94: 906-912, 1999.
15. Kato H, Kuwano H, Nakajima M, *et al*: Usefulness of positron emission tomography for assessing the response of neoadjuvant chemoradiotherapy in patients with esophageal cancer. Am J Surg 184: 279-283, 2002.
16. Brucher BL, Weber W, Bauer M, *et al*: Neoadjuvant therapy of esophageal squamous cell carcinoma; response evaluation by positron emission tomography. Ann Surg 233: 300-309, 2001.
17. Lowe SW, Bodis S, McClatchey A, *et al*: P53 status and the efficacy of cancer therapy *in vivo*. Science 266: 807-810, 1991.
18. Ikeguchi M and Maeta M: The expression of mutated p53 protein and proliferative activity of cancer cells in patients with esophageal squamous cell carcinoma. J Yonago Med Ass 49: 261-267, 1998.
19. Ikeguchi M, Sato H, Kitano K, *et al*: Radiochemosensitivity and expression of p53 in patients with esophageal cancer treated by avsolute non-curative resection. Anticancer Res 18: 493-498, 1998.
20. Kishi K, Doki Y, Miyata H, *et al*: Prediction of the response to chemoradiation and prognosis in oesophageal squamous cancer. Br J Surg 89: 597-603, 2002.
21. Imdahl A, Borgnar G, Schulte-Monting J, *et al*: Predictive factors for response to neoadjuvant therapy in patients with esophageal cancer. Euro J Card-thorac Surg 21: 657-663, 2002.
22. Okumura H, Natsugoe S, Yokomakura N, *et al*: The new criteria of clinical response for the primary tumor based on the findings of histological response after chemoradiation therapy in esophageal cancer. Jpn J Gastroenterol Surg 38: 1637-1644, 2005.

Vitamin K2-induced cell growth inhibition via autophagy formation in cholangiocellular carcinoma cell lines

MASANOBU ENOMOTO[1], AKIHIKO TSUCHIDA[1], KEISUKE MIYAZAWA[2], TOMOHISA YOKOYAMA[2], HIDEAKI KAWAKITA[1], HIROMI TOKITA[1], MUNEKAZU NAITO[3], MASAHIRO ITOH[3], KAZUMA OHYASHIKI[2] and TATSUYA AOKI[1]

[1]Third Department of Surgery, [2]First Department of Internal Medicine and [3]Department of Anatomy, Tokyo Medical University, Tokyo, Japan

Received August 9, 2007; Accepted September 17, 2007

Abstract. Vitamin K2 (MK4) has antitumor effects on various types of cancer cell lines *in vitro*, and its efficacy has also been reported in clinical applications for patients with leukemia, myelodysplastic syndrome, and hepatocellular carcinoma (HCC). However, details of the mechanism of the antitumor effects of MK4 remain unclear. In the present study, we examined the antitumor effects of MK4 on cholangiocellular carcinoma (CCC) cell lines and its mechanism of action using the HL-60 leukemia cell line that exerts MK4-induced cell growth inhibition via apoptosis induction and cell cycle arrest as a control. MK4 exerted dose-dependent antitumor effects on all three types of CCC cell lines. However, apoptosis occurred in a smaller percentage of cells and there was less cell cycle arrest compared with other cancer cell lines studied previously, which suggested slight MK4-induced cell growth inhibition via apoptosis induction and cell cycle arrest. On the contrary, histopathological fidings showed a large number of cells containing vacuoles in their cytoplasm, and electron microscopic findings showed a large number of cytoplasmic autophagosomes and autolysosomes. These findings suggested evidence of autophagy-related cell death. Fluorescence microscopy following acridine orange staining revealed an increase in the number of cytoplasmic acidic vesicular organelles characteristic of autophagy. Moreover, there were few cells forming autophagic vesicles in the control group, while the percentage of cells containing vacuoles in the MK4-treated group increased with the duration of culture. These results suggested that, unlike in leukemia, gastric cancer, HCC, and other cancer cells, the antitumor effects of MK4 on CCC cells are induced via autophagy formation.

Correspondence to: Dr Akihiko Tsuchida, Third Department of Surgery, Tokyo Medical University, 6-7-1 Nishi-Shinjuku, Shinjuku-ku, Tokyo 160-0023, Japan
E-mail: akibobo@hotmail.com

Key words: cholangiocellular carcinoma, vitamin K2, chemoprevention, autophagy

Introduction

Vitamin K2 (VK2) is a fat-soluble vitamin that plays a role in the synthesis of prothrombin in the liver and affects the clotting system. VK2 has been reported to exert *in vitro* antitumor effects on malignant cells of various types of cancers including acute myeloid leukemia (AML), lung cancer, gastric cancer, and hepatocellular carcinoma (HCC) (1-5). Clinical investigations have also reported on the efficacy of VK2 describing a decreased number of blastic cells associated with oral medication of VK2 in patients with post-myelodysplastic syndrome AML (6) and a decreased percentage of blastic cells, an increased number of mature neutrophils, and improvement in decreased red blood cells and platelets in patients with myelodysplastic syndrome (MDS) (7). Furthermore, in a randomized controlled study in HCC patients judged as in complete remission following various treatments who were divided into a VK2-treated group and non-treated group, the VK2-treated group had lower recurrence, with a 3-year accumulated recurrent rate of 65.5%, compared with a rate of 92.2% in the non-treated group (8). Although factors including cancer cell-induced apoptosis, cell cycle arrest, and induction of differentiation are believed to contribute to the mechanisms of these *in vitro* and *in vivo* antitumor effects of VK2 (1-4), details remain to be examined.

Homologues of vitamin K consist of natural-found vitamins K1 (phytonadione: VK1) and K2 (menaquinone: VK2), and chemically-synthesized vitamin K3 (menadione: VK3). In general, antitumor effects are greatest in VK3, followed by VK2, and VK1 is believed to have the smallest effects (5,9). Although VK3 is considered to exert a large antitumor effect (10), its safety has not been documented because of no clinical use. VK2 is denoted by menaquinone-n (MKn) according to the number of isoprenoid radicals that make up its side chain, and 14 of these (MK1-MK14) are found in nature. MK4 (menatetrenone), the VK2 used in the present study, has a geranylgeraniol radical as its side chain, which is clinically used for treatment of diseases such as osteoporosis and hypoprothrombinemia. Since VK2 has already been used in

many clinical applications with few side effects (11), it is expected to be promptly used for clinical applications in cancer treatment.

In recent years, attention has been drawn to autophagy, like apoptosis, as a programmed cell death (PCD) (12). Autophagy fundamentally refers to a process where cells enclose their own cell organelles with an isolated membrane and deliver them to lysosomes for degradation, serving as a nonspecific degradation mechanism of autologous proteins. Autophagy, when induced by various types of stresses such as starvation, forms and re-utilizes the amino acid pool. Autophagy is a biological phenomenon inherent in all eukaryotes essential for vital activities. For this reason, autophagy has been recognized as a cytoprotective mechanism for cells to protect themselves from extracellular stresses (13,14). Furthermore, since autophagy-related gene knock-out mice were reported to exhibit an increased risk of developing cancers, autophagy has also been recognized as a tumor suppressor (15,16). However, in a culture using cells in which autophagy-related genes were suppressed by siRNA and to which an autophagy inhibitor, 3-methyladenine (3-MA), was added, cytotoxic effects of some anticancer agents on cancer cells were diminished. Based on this result, the concept of caspase-independent cell death via autophagy, that is autophagic cell death (type II PCD), has been receiving increased attention (16-18).

We previously reported that VK2 has antitumor effects on cell lines of leukemia (1), MDS (19), lung cancer (2,3), and gastric cancer (4) via apoptosis induction and cell cycle arrest and that Bcl-2 overexpressed HL-60 cell lines by bcl-2 gene transfection (HL-60-bcl-2) are resistant to VK2-inducing apoptosis, but show differentiation-inducing effects via the induction of G1 arrest (1). We also reported that VK2 shows cancer protective effects in an experiment using hamster models of biliary carcinogenesis in pancreaticobiliary maljunction (20). However, the detailed mechanism of cancer inhibition of VK2 remains to be defined. In the present study, we performed experiments using cholangiocellular carcinoma cell lines to examine to what extent autophagy contributes to VK2-induced antitumor effects and their mechanism of action.

Materials and methods

Cell lines and reagents. VK2 (menaquinone-4: MK4) was supplied by Eisai Co. Ltd. (Tokyo, Japan). Three types of cholangiocellular carcinoma cell lines, TFK-1 (21), MEC (22), and HuCC-T1 (23), were provided by the Institute of Development, Aging and Cancer, Tohoku University (Sendai, Japan). The HL-60 leukemia cell line that exerts cell growth inhibition via apoptosis induction and cell cycle arrest with the addition of VK2 were used as a control (1).

All cell lines were cultured in RPMI-1640 medium (Gibco, Grand Island, NY, USA) with 10% FBS (Hyclone, Logan, UT, USA) in an atmosphere of 5% CO_2 air at 37°C. Adherent cholangiocellular carcinoma cell lines were treated and separated using a 0.25% trypsin and 0.02% EDTA solution during the logarithmic growth phase to form a cell suspension with an adjusted cell count of $5x10^4$ cells/ml for the following experiments.

Assessment of the cell growth inhibition in response to MK4. MK4 was added to each cell suspension ($5x10^4$ cells/ml) to obtain final concentrations of 0.1, 0.5, 1, 2, 5, 10, 20, 50, and 100 μM. The cell suspensions were placed on each 96-well tissue culture plate (BD Biosciences, Bedford, MA, USA) to make five samples of wells containing 100 μl of cell suspension for each concentration including the control group, and incubated for 96 h. After adding a 10 μl of reagent (5 mM WST-1, 20 mM HEPES, 1-methoxy PMS 5 ml) prepared using a cell counting kit (Dojindo Laboratories, Kumamoto, Japan) into each well, the optical density of each well was measured with a microplate reader equipped with a 450-nm filter to calculate the percentage of optical density for each concentration to the controls as the relative cell number.

Assessment of apoptosis induction. Cells undergoing apoptosis were assessed by flow cytometry using APO2.7 (clone 2.7 A6A3) mouse monoclonal antibody (mAb) (Immunotech, Marseille, France) that reacts to the 7A6 antigen expressed by cells undergoing apoptosis (19). Cultured cells were separated using a 0.25% trypsin and 0.02% EDTA solution and washed twice with PBS containing 5% FBS. Then, $1x10^5$ cells were placed in 0.5 ml of PBS containing 5% FBS and incubated with the addition of APO2.7 mAb and FITC-conjugated goat anti-mouse IgG mAb (Immunotech) for 30 min at 4°C. Immunofluorescence was analyzed by flow cytometry using an Epics XL2 flow cytometer (Coulter Japan, Tokyo, Japan) to compare the percentage of APO2.7-positive cells in each cell line between the MK4-treated group and the control group.

Cell cycle analysis. For each cell line, two groups, with and without the addition of 50 μM of MK4, were established and the cells were separated using a 0.25% trypsin and 0.02% EDTA solution after 96-h incubation. The cell suspensions were stained with a solution containing 1% propidium iodide (Sigma), 100 μg/ml digitonin, 0.01% NaN_3, 200 μg/ml RNase (Sigma), and 2.5% FBS for 10 min at room temperature, and fluorescence intensity of the cells were measured using a flow cytometer (Epics XL2 flow cytometer). Based on this result, the populations of the G0/G1, S, and G2/M phases were analyzed using a cell-cycle analysis program, MultiCycle AV (Phoenix Flow Systems, San Diego, CA, USA) (1).

Immunoblotting for detection of Bcl-2. After each of the TFK-1 cell lines and the HL-60 cell lines was lysed using a lysis buffer solution (10 mM Tris-HCl pH 7.8, 150 mM NaCl, 1% NP-40, 1 mM EDTA, 10% glycerol, 1 mM phanylmethylsulfonyl fluoride, 0.15 U/ml aprotinin, 10 mg/ml leupeptin, 100 mM sodium floride, 2 mM sodium orthovanadate), determination of protein concentration was performed with a protein assay kit (Bio-Rad, Richmond, CA, USA). After the TFK-1 and the HL-60 cell lines at the same cell count were spinned down, the same amount of lysis buffer solution was added and solubilization of protein was performed under the same conditions. Then, the solubilized solutions with equalized protein content and cell count were fractionated on 15% SDS-PAGE and blotted to an Immobilon-P membrane (Bio-Rad). After reacting to anti-human Bcl-2 mAb (BD Biosciences Pharmingen, San Jose,